**Smart Structures and Systems**, *Vol. 27, No. 1 (2021) 61-71*
DOI: https://doi.org/10.12989/sss.2021.27.1.061


# Vibration control of a smart piezo beam via gain scheduling H∞ controller based on LPV model

Abdullah Turan [1a], Melin Sahin*[2] and Cem Onat [3b]

[1] *Department of Mechanical Engineering, Inonu University, Malatya, Turkey*
[2] *Department of Aerospace Engineering, Middle East Technical University, Ankara, Turkey*
[3] *Department of Airframe and Power-plant, Firat University, Elazig, Turkey*

(*Received March 5, 2020, Revised November 11, 2020, Accepted November 17, 2020*)

**Abstract.** In this study, a gain scheduling $H_\infty$ controller based on Linear Parameter Varying (LPV) model was designed and applied to suppress the first out of plane bending vibration of a variable parameter smart beam equipped with Lead-Zirconium-Titanium (PZT) patches. This paper also introduces a novel LPV modelling technique which defalcates the zeros of the system. The controller design was carried out in three successive steps. In the first step, the variable parameter model of the beam with an added mass at its free end can rotate through a micro servo motor was experimentally obtained. In the second step, an original LPV model including the variable parameter model was obtained. Finally, $H_\infty$ controller with gain scheduling was designed on LPV model. The obtained controller was then used both for simulations and experimental verifications. It was shown that in response to parameter changes in the system, the proposed controller is capable of suppressing the beam bending vibrations by also exhibiting a robust performance. In practice, the proposed LPV controller design strategy can be transacted for vibration control of aircraft wings, the parameters of which vary according to various load conditions changing in time and therefore deeply affects the passive characteristics of the system of interest.

**Keywords:** smart beam; robust control; H∞; gain scheduling; LPV model

## 1. Introduction

Investigation and control of vibrations, in all structures where lightness and durability are targeted, is a very important issue. Developments in sensor and actuator technologies in recent years increase the use of smart structures in active vibration control applications in flexible mechanical systems. The most common type of piezoelectric materials (i.e., PZTs) are the piezo-ceramics. Piezo-ceramics can be adhered on flexible mechanical systems to obtain so-called smart structures (Avsar and Sahin 2016).

Researches on the design of controllers for active vibration control of smart beams can be classified into three categories as classical, adaptive and robust (Ros *et al*. 2015). Traditional controller applications such as Proportional-Integral-Derivative (PID) and Proportional-Derivative (PD) are among the most common working groups in the literature (Alam and Rahman 2010, *Chhabra et al*. 2012, Kumar *et al*. 2014, Khot *et al*. 2012). Traditional controllers, which stand out with their simplicity comprehensibility in structure, offer simple solutions for structures where high performance is not expected. However, additional challenging problems such as high performance expectations, uncertainties in the system model, and different operating conditions make traditional controllers inadequate in the vibration control of flexible structures. From this point of view, adaptive control algorithms can provide more suitable solutions (Shouwei *et al*. 2010, Saad *et al*. 2012, Zorić *et al*. 2014). However, the adaptive control architectures require an adaptation scheme in addition to the adjustable controller structure by making the controller structure quite complicated. In addition to this, in practice, it takes a certain time for the change in operating conditions to vary the system parameters and to adapt the controller into this new state. The process of adapting the controller to the changes in the operating conditions leads to significant performance losses. Controllers designed with robust control methods should be used to control beam vibrations with a single Linear Time Invariant (LTI) controller without loss of a performance despite the uncertainties in both parameters and the modelling of in the system. On the other hand, robust control, in addition to the external inputs of the system, focuses on the compromise between performance and stability in the presence of both non-linearities and parameter uncertainties in the system model (Onat *et al*. 2007, 2019, Onat 2015, Algermissen *et al*. 2009). Several controllers comprising $H_\infty$ (Sahin *et al*. 2008, Omidi and Mahmoodi 2014, Oveisi and Nestorovic 2014), PID (*Kumar et al*. 2014), Linear Quadratic Regulator (LQR) (Onat *et al*. 2011a, Akın and Sahin 2017), Continued Fraction Expansion (CFE) (Onat *et al*. 2012) and LPV (Onat *et al*. 2011b) were designed in order and then their performances

*Corresponding author, Ph.D., Associate Professor, E-mail: msahin@metu.edu.tr
[a] Ph.D. Student, E-mail: abdullah.turan@inonu.edu.tr
[b] Ph.D., Associate Professor, E-mail: conat@firat.edu.tr



ISSN: 1738-1584 (Print), 1738-1991 (Online)

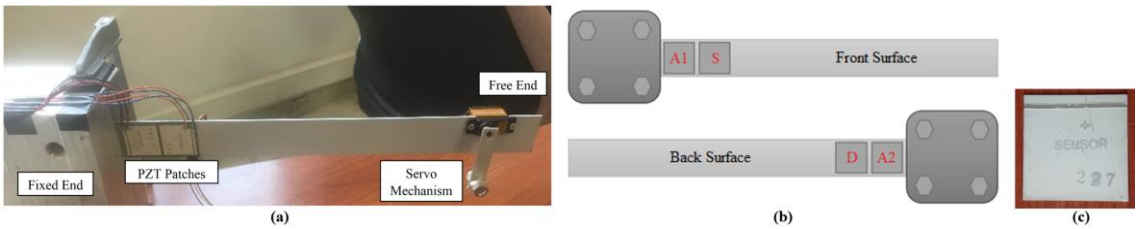


Fig. 1 (a) Smart beam; (b) Labels of the PZT patches; (c) PZT patch (BMP500) (Akın 2015)

were examined and compared to achieve an active vibration damping on the smart beam.

Since the cantilever beam model used in aforementioned studies having fixed mass and strength properties, it is insufficient to represent the changes in the physical parameters of the system in real case scenarios where the system parameters mostly vary depending on the operating conditions. For example, as although the cantilever aluminum beam easily can be handled in experimental studies, the natural frequencies and vibration patterns of an aircraft wing change as the fuel stored in aircraft wings is used or as the outside temperature changes over a wide range. Akın added an extra mass to the free end of the beam with an arm that can be repositioned via a micro servo motor (Akın 2015). His aim is to reflect the change in the physical properties of the system to the experimental model and to model the real case scenario in a larger domain. Accordingly, the system model can be predictably altered with help of the servo motor through an arm holding the mass at 5 different angles. In this study, it was observed that the performance of the LQR controller was not adequate for all cases and robustness was then provided by also using an artificial neural network control algorithm. In another study, a controller design was presented for the smart beam model with varying parameters (Onat *et al*. 2017). The authors designed a gain-scheduling $H_\infty$ controller using a perturbation model covering the analytical model of the smart beam in all cases.

In this research study on the other hand, $H_\infty$ controller with gain scheduling based on LPV model is designed and applied to the so-called smart beam in order to suppress the vibration at its fundamental resonance frequency. For this purpose, an original LPV model covering the frequencies in the range of in all operating conditions is proposed and the gain-scheduling $H_\infty$ controller is designed by using the proposed LPV model. In this context, the proposed controller design provides an innovation and superiority over the other robust $H_\infty$ controller designs in the literature as;

- The controller design is based on the LPV model, which is also based on the experimental models of a smart beam with direct parameter varying.
- No reduction is performed for the application of the synthesized controller in the system model.
- No additional compensator is utilized for a performance increase.

The motivation of this study is to design and implement a controller which is sensitive to various angle changes of a servomechanism connected to the free end of a smart cantilever beam responsible from the tip mass variation. Experimental studies conducted both in time and frequency domains for five different cases show that the designed $H_\infty$ controller can handle control the effects of the change in the physical system by performing effectively in all defined operating conditions. This study consists of six sections. In Section 2, the smart beam model with parameter uncertainty and the proposed LPV model are presented. The design procedure of the LPV controller is then given in Section 3. The simulation and the experimental results are presented in Sections 4 and 5, respectively. The conclusions are drawn in Section 6.

## 2. Beam model with varying parameters

Fig. 1(a) shows the smart beam used in the study. The dimensions of this aluminium cantilever beam are 350 × 30 × 2 mm with four BM500 PZT patches having dimensions of 25.4 × 25.4 × 0.50 mm stuck in bimorph condition. The PZT patches are located as two on the front and two on the back surface configuration. These PZT patches are entitled as A1, A2, D, and S according to their intended use in Fig. 1(b). A1 and A2 are used as control PZT patches (i.e., actuators) and are connected in bimorph configuration. S and D stands for the sensor the disturbance given to the PZT patches, respectively. For bimorph configuration of the actuators, the cables which are then soldered on (A1) and (A2) are connected with opposite polarization (– of A1 with + of A2, + of A1 with – of A2) so that an applied voltage causes one of the piezoelectric patch to expand and the other to contract. By giving an initial displacement to the tip of the beam, the amplitude and the continuousness of the wave is observed for each piezoelectric patch (Akın 2015).

Experimental setup consists of the smart beam, a data acquisition system, an amplification system, and a sensor system which is described schematically in Fig. 2. The data acquisition system includes a host PC and a “Speedgoat Education Real-Time Target Machine (2020)” which is a high-performance real-time simulation and testing platform where the control algorithm is embedded. Since PZT patches need high voltage for effective usage, a high-voltage amplifier (Sensor Technology SA10, 2020) is installed to use both for disturbance and bimorph actuator signals.

The physical parameter changes in the system are taken into account in the experimental model by means of different values of the angle ($\Theta$) that the servo mechanism arm makes with the vertical axis. Servo arm can be changed between +64° and –64° as shown in Fig. 3. Accordingly, the

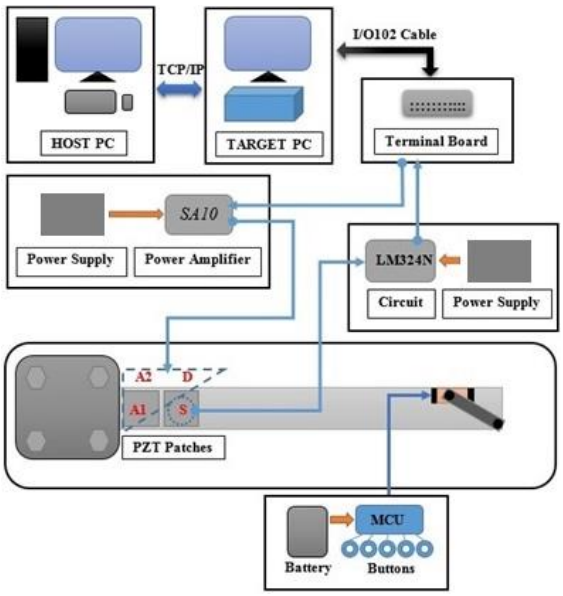


Fig. 2 Experimental setup

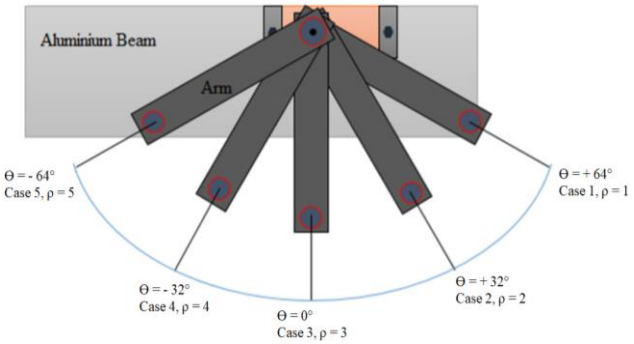


Fig. 3 Different arm configurations

first servo arm angle is +64°, the second case is at +32°, the third case is taken as 0°, the fourth case is at –32° and the fifth case is at –64°. With this pairing, the position of the servo arm is indicated by ρ. The range of Θ is (+64°, –64°) and therefore it corresponds to a change in range of ρ as Eqs. (1)-(5).

For each of the above-mentioned positions, a chirp sine wave in the range of 5 Hz to 30 Hz is given through the actuator PZT patches and the system response is measured by using the PZT patch nominated as a sensor. The input-output data are converted to frequency response function by means of an FFT using MATLAB computer program. Then, state-space models for five different positions are obtained from the frequency response functions. These, state-space models for 5 different cases are given in Eqs. (1)-(5), respectively.

$$A_{G1} = \begin{bmatrix} -1.5255 & -7193.2 \\ 1 & 0 \end{bmatrix}, \quad B_{G1} = \begin{bmatrix} 1 \\ 0 \end{bmatrix}, \quad C_{G1} = [0.3432 \quad 120.208], \quad D_{G1} = [0.0182] \tag{1}$$

$$A_{G2} = \begin{bmatrix} -1.584 & -7604.7 \\ 1 & 0 \end{bmatrix}, \quad B_{G2} = \begin{bmatrix} 1 \\ 0 \end{bmatrix}, \quad C_{G2} = [0.3644 \quad 130.5907], \quad D_{G2} = [0.0176] \tag{2}$$

$$A_{G3} = \begin{bmatrix} -1.675 & -8175.1 \\ 1 & 0 \end{bmatrix}, \quad B_{G3} = \begin{bmatrix} 1 \\ 0 \end{bmatrix}, \quad C_{G3} = [0.39 \quad 144.87], \quad D_{G3} = [0.0169] \tag{3}$$

$$A_{G4} = \begin{bmatrix} -1.7759 & -8796.6 \\ 1 & 0 \end{bmatrix}, \quad B_{G4} = \begin{bmatrix} 1 \\ 0 \end{bmatrix}, \quad C_{G4} = [0.4171 \quad 160.8472], \quad D_{G4} = [0.0162] \tag{4}$$

$$A_{G5} = \begin{bmatrix} -1.8454 & -9216.7 \\ 1 & 0 \end{bmatrix}, \quad B_{G5} = \begin{bmatrix} 1 \\ 0 \end{bmatrix}, \quad C_{G5} = [0.4332 \quad 171.68], \quad D_{G5} = [0.0158] \tag{5}$$

The state space model of beam with parameter varying can be given in the general form as in Eq. (6). Here, the variable specified ρ is the position of the servo arm.

$$A(\rho) = \begin{bmatrix} -\rho_1(\rho) & -\rho_2(\rho) \\ 1 & 0 \end{bmatrix}, \quad B = \begin{bmatrix} 1 \\ 0 \end{bmatrix}, \quad C(\rho) = [\rho_3(\rho) \quad \rho_4(\rho)], \quad D(\rho) = [\rho_5(\rho)] \tag{6}$$

Accordingly, five parameters ($\rho_1$, $\rho_2$, $\rho_3$, $\rho_4$ and $\rho_5$) change in the state space model together with the position of the servo arm. Variations of the parameters $\rho_1$, $\rho_2$, $\rho_3$, $\rho_4$ and $\rho_5$ by servo arm position are given in Fig. 4 in the experimental models given in Eqs. (1)-(5).

Here, it is observed that system parameters $\rho_1$, $\rho_2$, $\rho_3$, $\rho_4$ and $\rho_5$ change linearly with great sensibility with servo arm position ρ and the relations given in Eqs. (7)-(11) and summarized in Table 1.

$$\rho_1(\rho) = 0.08317\rho + 1.432 \tag{7}$$

$$\rho_2(\rho) = 523.9\rho + 6626 \tag{8}$$

$$\rho_3(\rho) = 0.02327\rho + 0.3198 \tag{9}$$

$$\rho_4(\rho) = 13.32\rho + 105.7 \tag{10}$$

$$\rho_5(\rho) = -0.00062\rho + 0.0188 \tag{11}$$

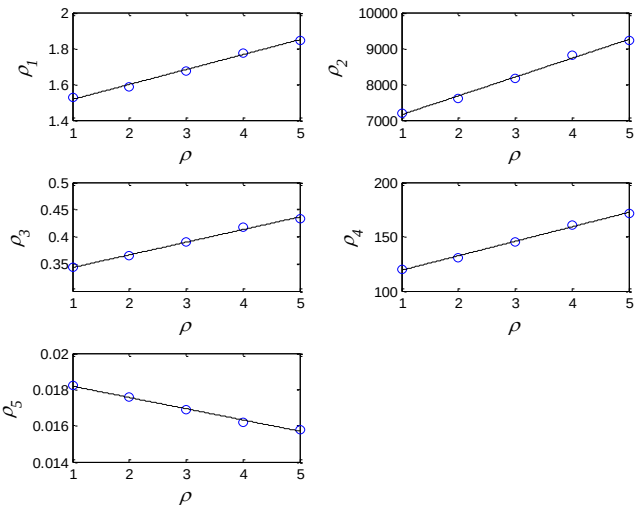


Fig. 4 Variation of experimental state-space model parameters with servo arm position (ρ)

Table 1 The relationship of system parameters with ρ and its regression coefficients

| Fitted relation | Regression coefficient ($R^2$) |
|---|---|
| $\rho_1(\rho) = 0.08317\rho + 1.432$ | 0.9931 |
| $\rho_2(\rho) = 523.9\rho + 6626$ | 0.9951 |
| $\rho_3(\rho) = 0.02327\rho + 0.3198$ | 0.9944 |
| $\rho_4(\rho) = 13.32\rho + 105.7$ | 0.9950 |
| $\rho_5(\rho) = -0.00062\rho + 0.0188$ | 0.9928 |

If Eqs. (7)-(11) and Eq. (6) are evaluated together, Eq. (12) is obtained.

$$\begin{aligned} A(\rho) &= \begin{bmatrix} \text{-0.08317}\rho\text{-1.432} & \text{-523.9}\rho\text{-6626} \\ 1 & 0 \end{bmatrix}, \\ B &= \begin{bmatrix} 1 \\ 0 \end{bmatrix}, \\ C(\rho) &= [\ 0.02327\rho+0.3198 \quad 13.32\rho+105.7\ ], \\ D(\rho) &= [\ \text{-0.00062}\rho+0.0188\ ] \end{aligned} \tag{12}$$

Considering the linear state-space model together with ρ, the following LPV model of the system can be constructed as

$$A(\rho) = A_0 + \rho A_1, \tag{13}$$

$$B = B_0, \tag{14}$$

$$C(\rho) = C_0 + \rho C_1, \tag{15}$$

$$D(\rho) = D_0 + \rho D_1. \tag{16}$$

The matrices $A_0$, $B_0$, $C_0$ and $D_0$ are the constant parts of the system equations which do not depend on the scheduling parameters. $A_1$, $B_1$, $C_1$ and $D_1$ are, on the other hand, the matrices associated with the scheduling parameter. The open loop frequency response of the LPV model of the beam with parameter varying is given in Fig. 5. The resonance and anti-resonance frequencies vary with the intervals of the servo arm position (1-5) in the frequency range of [14.3-16.0] Hz and [15.0-22.0] Hz, respectively.

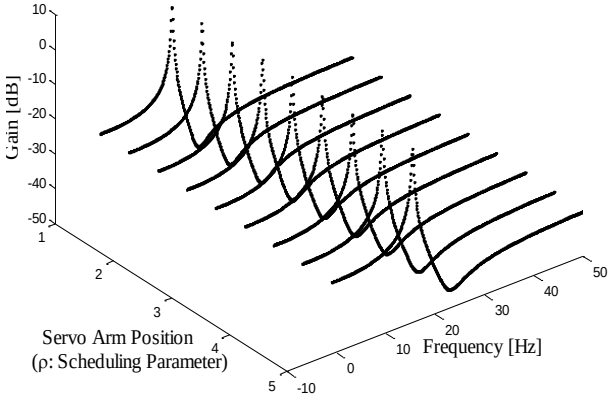


Fig. 5 Open loop frequency response of the beam with parameter varying

## 3. Design of the LPV controller

Note that the C and the D matrices of the LPV model obtained contain variable parts. In order to implement the LPV model-based gain scheduling controller design methodology, it is necessary to take these matrices constant at suitable value (Onat *et al*. 2007) approximately, or to take into account the denominator part of the controller after calculating the controller, not taking into account the polynomial in the numerator part of the transfer model function. From the study (Onat *et al*. 2007), the average of the extreme values of the C and D matrices are taken. The second method is pole-zero cancelation manipulation and in the proposed control design, the second method is used with constant C and D matrices.

**Remark:** The experimentally obtained system transfer function for the first position of the servo arm is given in Eq. (17). The state-space representation of the transfer function is given in Eq. (1).

$$G(s) = \frac{E_1(s)}{F_1(s)} = \frac{0.0182s^2 + 0.3710s + 251.1245}{s^2 + 1.5255s + 7193.2} \tag{17}$$

The manipulation process is illustrated using the basic control block diagram in Fig. 6 for LTI systems. Here K(s) refers to the controller transfer function. E(s) and F(s) is the numerator and denominator part of the system transfer function, respectively. Note that the closed-loop systems are completely equivalent to each other. The same manipulation can be performed for LPV systems as shown in Fig. 7.

Note that this manipulation process or the approach proposed by Onat *et al*. (2007) is not a preference for LPV-based controller design but it is a necessity due to the fact that the C and D matrices are constant. The proposed controller design is carried out in two steps. The first step is to design the LPV model over the experimental model of which numerator part is neglected (i.e., C and D matrices are fixed) and then calculate the gain scheduling controller. The second step is to take the dynamics of the numerator polynomial of the system model neglected in the first stage of the design in the denominator part of the controller dynamics into account. For this purpose, in the first phase of the controller design, the form of the manipulated state variable space for different servo arm positions is provided in Eqs. (18)-(22).

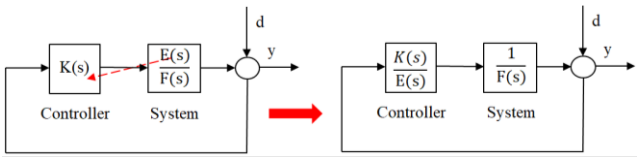


Fig. 6 Manipulation for LTI equivalent systems

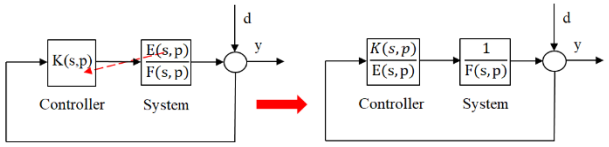


Fig. 7 Manipulation for LPV systems

$$A_{Gm1} = \begin{bmatrix} -1.5255 & -7193.2 \\ 1 & 0 \end{bmatrix}, \quad B_{Gm1} = \begin{bmatrix} 1 \\ 0 \end{bmatrix}, \quad C_{Gm1} = [0 \quad 1], \quad D_{Gm1} = [0] \tag{18}$$

$$A_{Gm2} = \begin{bmatrix} -1.584 & -7604.7 \\ 1 & 0 \end{bmatrix}, \quad B_{Gm2} = \begin{bmatrix} 1 \\ 0 \end{bmatrix}, \quad C_{Gm2} = [0 \quad 1], \quad D_{Gm2} = [0] \tag{19}$$

$$A_{Gm3} = \begin{bmatrix} -1.675 & -8175.1 \\ 1 & 0 \end{bmatrix}, \quad B_{Gm3} = \begin{bmatrix} 1 \\ 0 \end{bmatrix}, \quad C_{Gm3} = [0 \quad 1], \quad D_{Gm3} = [0] \tag{20}$$

$$A_{Gm4} = \begin{bmatrix} -1.7759 & -8796.6 \\ 1 & 0 \end{bmatrix}, \quad B_{Gm4} = \begin{bmatrix} 1 \\ 0 \end{bmatrix}, \quad C_{Gm4} = [0 \quad 1], \quad D_{Gm4} = [0] \tag{21}$$

$$A_{Gm5} = \begin{bmatrix} -1.8454 & -9216.7 \\ 1 & 0 \end{bmatrix}, \quad B_{Gm5} = \begin{bmatrix} 1 \\ 0 \end{bmatrix}, \quad C_{Gm5} = [0 \quad 1], \quad D_{Gm5} = [0] \tag{22}$$

With the proposed manipulation process, the matrices A and B remain the same and the matrices C and D are as constant. Accordingly, only the two parameters $\rho_1$ and $\rho_2$ in the system matrix A change with the servo arm position ρ. The variation of $\rho_1$ and $\rho_2$ with ρ is given previously in Eqs. (7) and (8).

The manipulated state-space model of the parameter variable beam can be given in the general form as in Eq. (23). $A_m$, $B_m$, $C_m$ and $D_m$ are the system matrices.

$$A_m(\rho) = \begin{bmatrix} -\rho_1(\rho) & -\rho_2(\rho) \\ 1 & 0 \end{bmatrix}, \quad B_m = \begin{bmatrix} 1 \\ 0 \end{bmatrix}, \quad C_m = [0 \quad 1], \quad D_m = [0] \tag{23}$$

When Eqs. (7) and (8) are evaluated together with Eq. (23), the Eq. (24) can be obtained.

$$\tilde{A}(\rho) = \begin{bmatrix} \text{-0.08317}\rho\text{-1.432} & \text{-523.9}\rho\text{-6626} \\ 1 & 0 \end{bmatrix}, \quad \tilde{B} = \begin{bmatrix} 1 \\ 0 \end{bmatrix}, \quad \tilde{C} = [0 \quad 1], \quad \tilde{D} = [0] \tag{24}$$

Considering the manipulated linear state-space model together with the scheduling parameter (ρ: servo arm position), the following LPV model of the system in Eqs. (25)-(28) can be readily constructed for the gain scheduling controller design

$$\tilde{A} = \tilde{A}_0 + \rho\tilde{A}_1, \tag{25}$$

$$\tilde{B}_u = \tilde{B}_w = \begin{bmatrix} 1 \\ 0 \end{bmatrix}, \tag{26}$$

$$\tilde{C}_e = \tilde{C}_y = [0 \quad 1] \tag{27}$$

$$\tilde{D}_{ew} = \tilde{D}_{eu} = \tilde{D}_{yw} = \tilde{D}_{yu} = [0] \tag{28}$$

Here, $\tilde{A}$ is the system matrix, $\tilde{B}_u$ is the control input matrix, $\tilde{B}_w$ is the disturbance input matrix, $\tilde{C}_e$ is the output matrix for the performances, $\tilde{C}_y$ is the measurement matrix, $\tilde{D}_{ew}$ is the arm position input scaling matrix for the performance outputs, $\tilde{D}_{yw}$ is the arm position input matrix for the measurement outputs, $\tilde{D}_{eu}$ is the control input matrix for the performance outputs, and $\tilde{D}_{yu}$ is the control input matrix for the measurements. The matrix $\tilde{A}_0$ is the constant part of the system matrix which do not depend on the scheduling parameters and it is given in Eq. (29). $\tilde{A}_1$ is the matrix associated with the ρ scheduling parameter and it is given in Eq. (30).

$$\tilde{A}_0 = \begin{bmatrix} -1.432 & -6626 \\ 1 & 0 \end{bmatrix} \tag{29}$$

$$\tilde{A}_1 = \begin{bmatrix} -0.08317 & -523.9 \\ 1 & 0 \end{bmatrix} \tag{30}$$

The block diagram for the augmented plant is shown in Fig. 8. Here $e_1$ and $e_2$ are the performance outputs. For these outputs, two output weighting filters are assigned as $W_s$ and $W_{act}$ are associated with the closed loop performance (y) and the restriction of control signal (u), respectively. The dynamic scaling weight chosen to be associated with the external disturbance caused the vibration is taken as $W_r$. Finally, the static weight assigned to sensor noise is assigned as $W_n$. These filters are respectively given in Eqs. (31)-(34).

$$W_S(s) = \frac{120s}{s^2 + 120s + 14400} \tag{31}$$

$$W_{act}(s) = \frac{6s}{s^2 + 120s + 14400} \tag{32}$$

$$W_r(s) = \frac{3760}{s + 80} \tag{33}$$

$$W_n(s) = \frac{120s}{s^2 + 120s + 14400} \tag{34}$$

The state-space representation of the augmented plant and the controller are given in Eqs. (35) and (36).

$$\begin{bmatrix} \dot{x}(t) \\ e(t) \\ y(t) \end{bmatrix} = \begin{bmatrix} \tilde{A}(\rho(t)) & \tilde{B}_w & \tilde{B}_u \\ \tilde{C}_e(\rho(t)) & \tilde{D}_{ew} & \tilde{D}_{eu} \\ \tilde{C}_y & \tilde{D}_{yw} & \tilde{D}_{yu} \end{bmatrix} \begin{bmatrix} x(t) \\ d(t) \\ u(t) \end{bmatrix} \tag{35}$$

$$\begin{bmatrix} \dot{x}_K \\ u \end{bmatrix} = \begin{bmatrix} A_K(\rho(t)) & B_K(\rho(t)) \\ C_K(\rho(t)) & D_K(\rho(t)) \end{bmatrix} \begin{bmatrix} x_K \\ y \end{bmatrix} \tag{36}$$

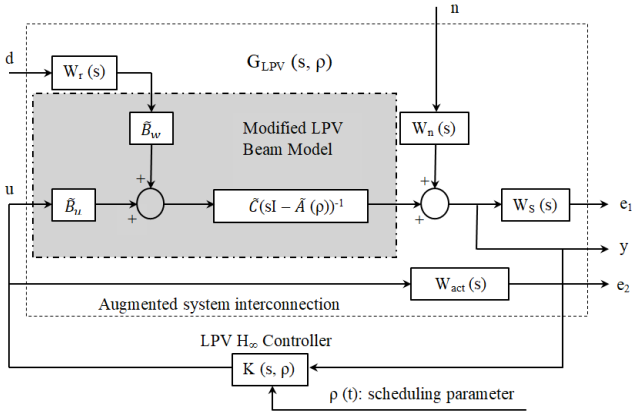


Fig. 8 The augmented system

where $x_K(t)$ is the state vector, u(t) is the control vector, y(t) is the measurement vector, e(t) is performance output vector and d(t) is the disturbance.

Note that the only matrices in Eq. (35) that are associated with the scheduling vector ρ are A and $\tilde{C}_e$. The quadratic LPV-γ problem is then solved to find the $A_K(\rho)$, $B_K(\rho)$, $C_K(\rho)$ and $D_K(\rho)$ controller matrices, of dimensions (m x m), (m x $n_y$), ($n_u$ x m) and ($n_u$ x $n_y$), respectively and a minimum value of γ so that the closed loop system is stable and the $L_2$ induced norm of the transfer function from d to e stays less than γ for all values of $\rho(t) \in \Gamma$.

Here, m is the dimension of the controller state vector, n is the dimension of the plant state space, $n_y$ is the dimension of the measurement space and $n_u$ is the dimension of the control space. This problem is feasible if and only if a common symmetric $W > 0$ of dimension (n + m) × (m + n) exists such that

$$\begin{bmatrix} A_{cli}^T(\rho)W + WA_{cli}(p) & WB_{cli}(p) & \gamma^{-1}B_{cli}^T(\rho) \\ B_{cli}^T(\rho)W & -I & \gamma^{-1}D_{cli}^T(\rho) \\ \gamma^{-1}C_{cli}(\rho) & \gamma^{-1}D_{cli}(\rho) & -I \end{bmatrix} < 0 \quad (37)$$

$i = 1, \dots, r$

holds for all $\rho(t) \in \Gamma$ where Γ is the convex polytope of corners $\Gamma_1, \Gamma_2, \dots, \Gamma_r$; that is

$$\Gamma = \left\{ \sum_{i=1}^{r} \lambda_i \Gamma_i : \lambda_i \geq 0; \quad \sum_{i=1}^{r} \lambda_i = 1 \right\} \quad (38)$$

where $A_{cli}$, $B_{cli}$, $C_{cli}$ and $D_{cli}$ are the closed-loop system matrices at the $i^{th}$ vertex. It can be shown that finding a common symmetric solution $W > 0$ to Eq. (37) at each vertex point $(\Gamma_i | i = 1, \dots, r)$ can be reduced to track the common symmetric matrices $R > 0$ and $S > 0$ such that

$$N_R^T \begin{bmatrix} \tilde{A}_i R + R\tilde{A}_i^T & R\tilde{C}_{ei}^T & \tilde{B}_{wi} \\ * & -\gamma I & \tilde{D}_{ew} \\ * & * & -\gamma I \end{bmatrix} N_R < 0 \quad i = 1, , r \quad (39)$$

$$N_S^T \begin{bmatrix} \tilde{A}_i^T S + S\tilde{A}_i & S\tilde{B}_{wi} & \tilde{C}_{ei}^T \\ * & -\gamma I & \tilde{D}_{ew}^T \\ * & * & -\gamma I \end{bmatrix} N_S < 0 \quad i = 1, , r \quad (40)$$

$$\begin{bmatrix} R & I \\ I & S \end{bmatrix} \geq 0 \quad (41)$$

holds. Here, $N_R$ and $N_S$ denote bases for the null spaces of $(\tilde{B}_u^T, \tilde{D}_{eu}^T)$ and $(\tilde{C}_y, \tilde{D}_{yw})$, respectively. It is then straightforward to construct the corner controllers using the elimination lemma (Boyd *et al.* 1994). Let us denote the controller associated with the $i^{th}$ vertex with

$$\Omega_i \triangleq \begin{bmatrix} A_{ci} & B_{ci} \\ C_{ci} & D_{ci} \end{bmatrix} \quad (42)$$

Then, the controller for any value of $\rho(t) \in \Gamma$ would be

$$\Omega_\rho \triangleq \begin{bmatrix} A_c(\rho) & B_c(\rho) \\ C_c(\rho) & D_c(\rho) \end{bmatrix} = \sum_{i=1}^{r} \lambda_i \Omega_i \quad (43)$$

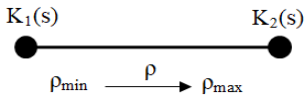


Fig. 9 The corner controllers and their convex space

where $(\lambda_1, \lambda_2, \dots, \lambda_r)$ is any solution of convex decomposition problem given in Eq. (38).

Gain scheduling controllers operate by switching between the pre-calculated LTI controllers for various operating points using a common Lyapunov function depending on the measurement of the scheduling parameter. In this research control problem, it is assumed that there is one scheduling parameter, thus the number of vertices is 2. In other words, there are two corner controllers. Transfer functions of the corner controllers are $K_1(s)$ and $K_2(s)$. Hence, two local controllers are designed for different values of ρ. Fig. 9 shows the vertices of the corresponding polytope and the associated vertex controllers. The corner controllers $K_1(s)$ and $K_2(s)$ are the controllers for the first and fifth positions of the servo arm, respectively. Remember that ρ is defined in the range (1-5), where $\rho_{min}$ = 1 (i.e., +64° position of the servo arm) and $\rho_{max}$ = 5 (i.e., -64° position of the servo arm).

In the first stage of the design, the design process is completed when the numerator part of the transfer function at the boundary positions (i.e., for ρ = 1 and ρ = 5) of the neglected system is properly taken into account in the controller transfer function. According to this, the state-space models of the corner controllers calculated (i.e., $K_1(s)$ and $K_2(s)$) are $A_{K1}$, $B_{K1}$, $C_{K1}$, $D_{K1}$ and $A_{K2}$, $B_{K2}$, $C_{K2}$, $D_{K2}$, respectively and the state-space model matrices ($A_K(\rho)$, $B_K(\rho)$, $C_K(\rho)$ and $D_K(\rho)$) of the gain scheduling $H_\infty$ controller can be written as in Eqs. (44)-(47).

$$A_K(\rho) = A_{K1} + \frac{\rho - \rho_{min}}{\rho_{max} - \rho_{min}}(A_{K2} - A_{K1}) \quad (44)$$

$$B_K(\rho) = B_{K1} + \frac{\rho - \rho_{min}}{\rho_{max} - \rho_{min}}(B_{K2} - B_{K1}) \quad (45)$$

$$C_K(\rho) = C_{K1} + \frac{\rho - \rho_{min}}{\rho_{max} - \rho_{min}}(C_{K2} - C_{K1}) \quad (46)$$

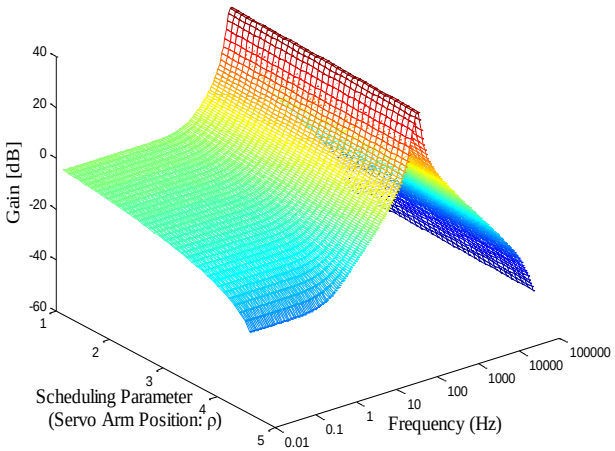


Fig. 10 The frequency response of the controller

$$D_K(\rho) = D_{K1} + \frac{\rho - \rho_{min}}{\rho_{max} - \rho_{min}}(D_{K2} - D_{K1}) \quad (47)$$

The frequency response dependent on the scheduling parameter ρ of the designed $H_\infty$ controller with gain scheduling is given in Fig. 10. The gain scheduling parameter increases while the controller gain decreases in all frequency zones. The controller is particularly effective for all scheduling parameter values around the resonance frequency of the system.

## 4. Results of the simulations

Simulation studies are performed in both time and frequency domains. Fig. 11 shows the time domain free vibration responses of the smart beam for five different cases (i.e., arm positions). Studies are performed in Matlab/Simulink environment with five different corner controllers determined for five arm positions. Here, sine wave inputs are used in the first resonance frequencies (13.5, 13.85, 14.38, 14.92 and 15.3 Hz), for cases of one to

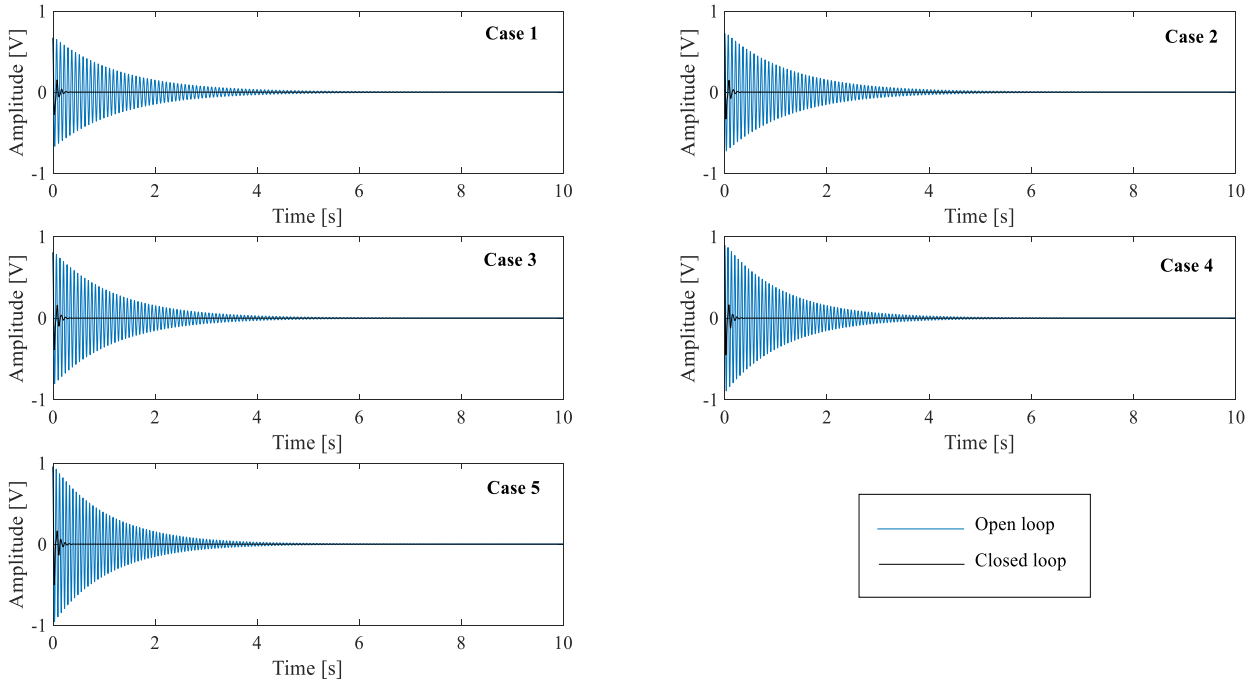


Fig. 11 Time domain free vibration responses of the smart beam

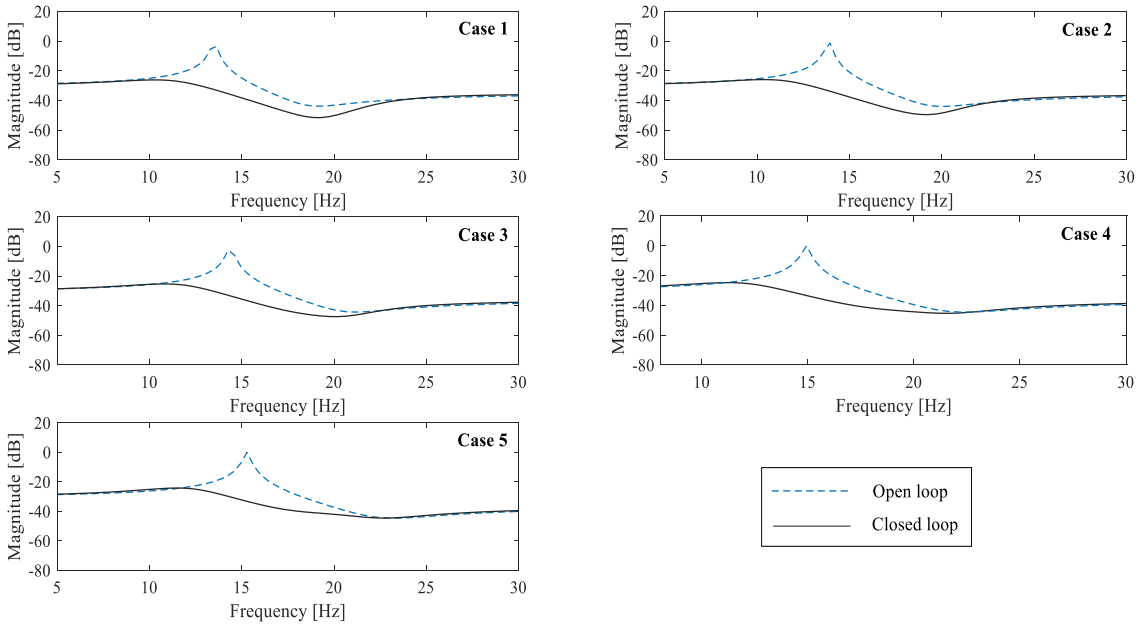


Fig. 12 Frequency domain vibration responses of the smart beam

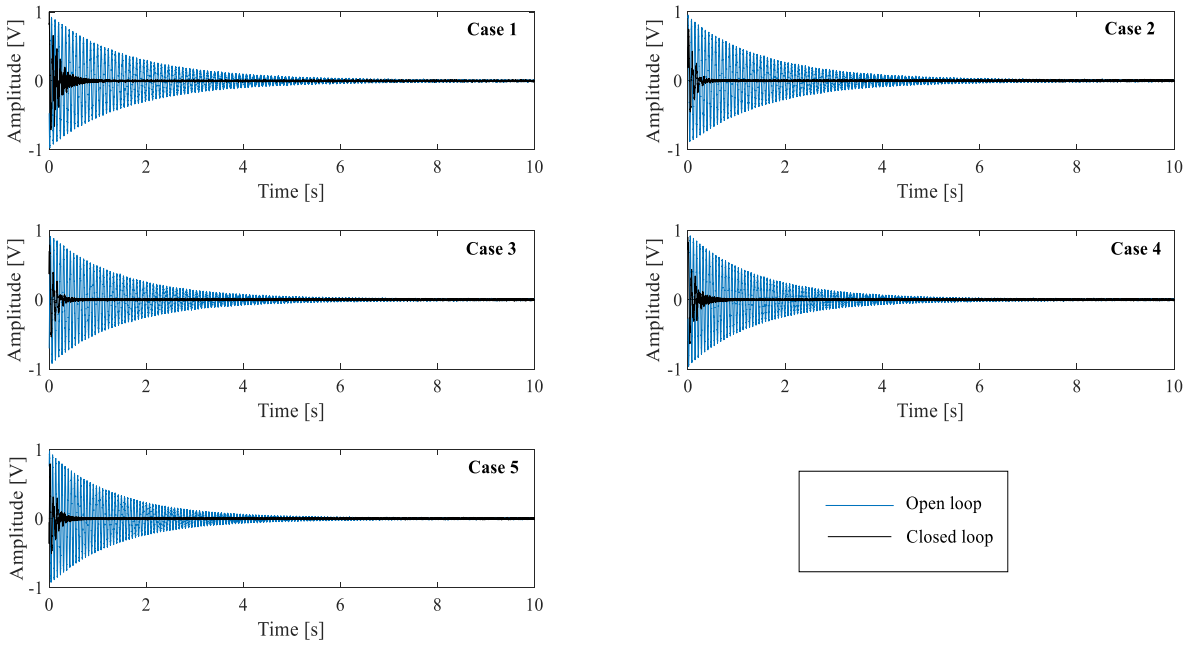


Fig. 13 Time domain free vibration responses of the smart beam

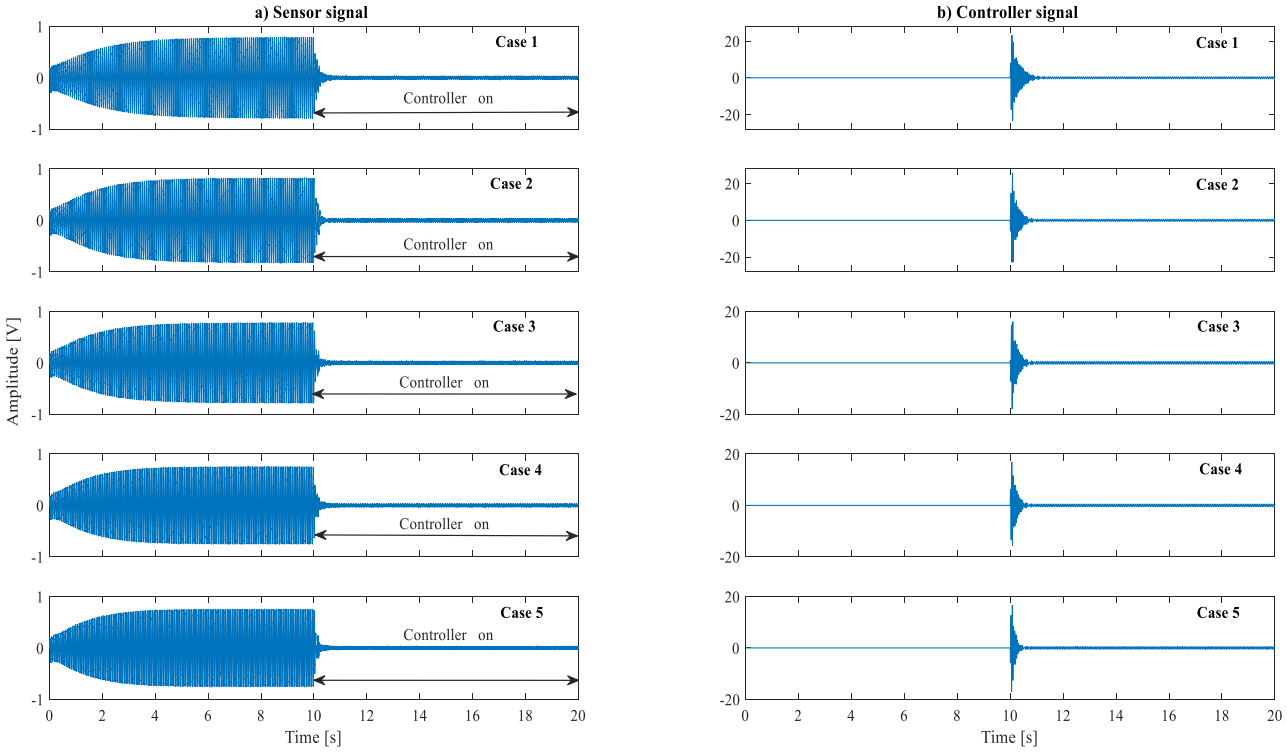


Fig. 14 (a) Time domain forced vibration responses of the smart beam; (b) Controller output voltage

five in the simulation diagram, respectively. It can easily be observed from the Fig. 10 that the settling time is around 5 s for the open loop system. On the other hand, the designed controller managed to suppress the free vibrations of the smart beam with a settling time of nearly 0.5 s at around the first resonance region. Approximately the same level of vibration suppression performance is achieved for all cases. Fig. 12 shows the forced responses in the frequency domain for five different cases. Accordingly, the designed controller is capable of effectively suppressing the beam bending vibrations in the first resonance region for all cases by nearly 27 dB.

## 5. Experimental verification

Fig. 13 shows the experimental responses of the smart beam in the case of free vibration. The initial displacement

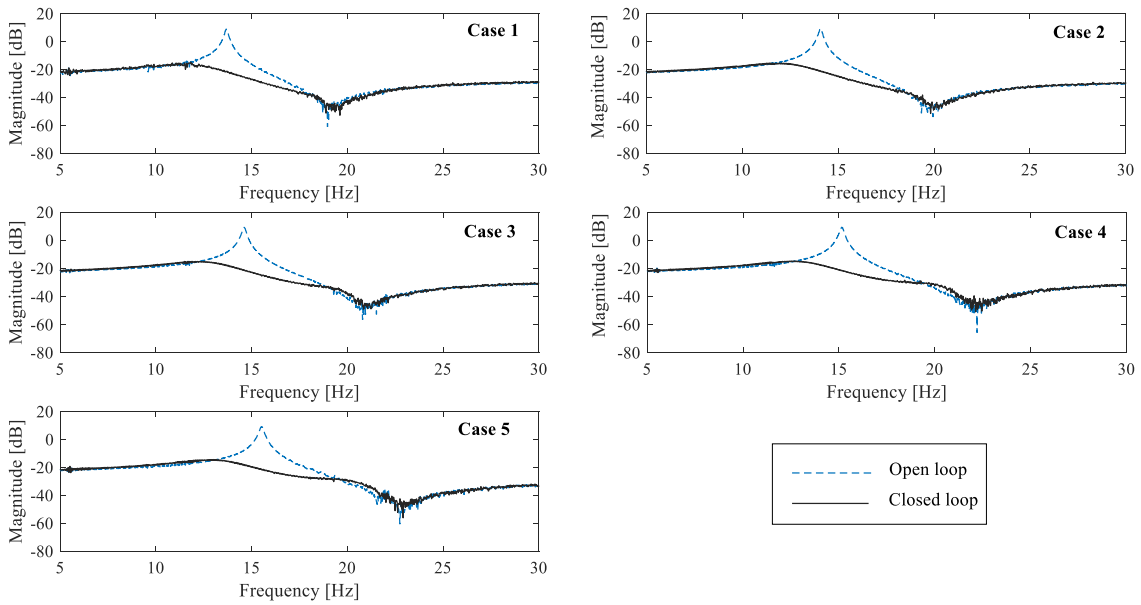


Fig. 15 Frequency domain responses of the smart beam

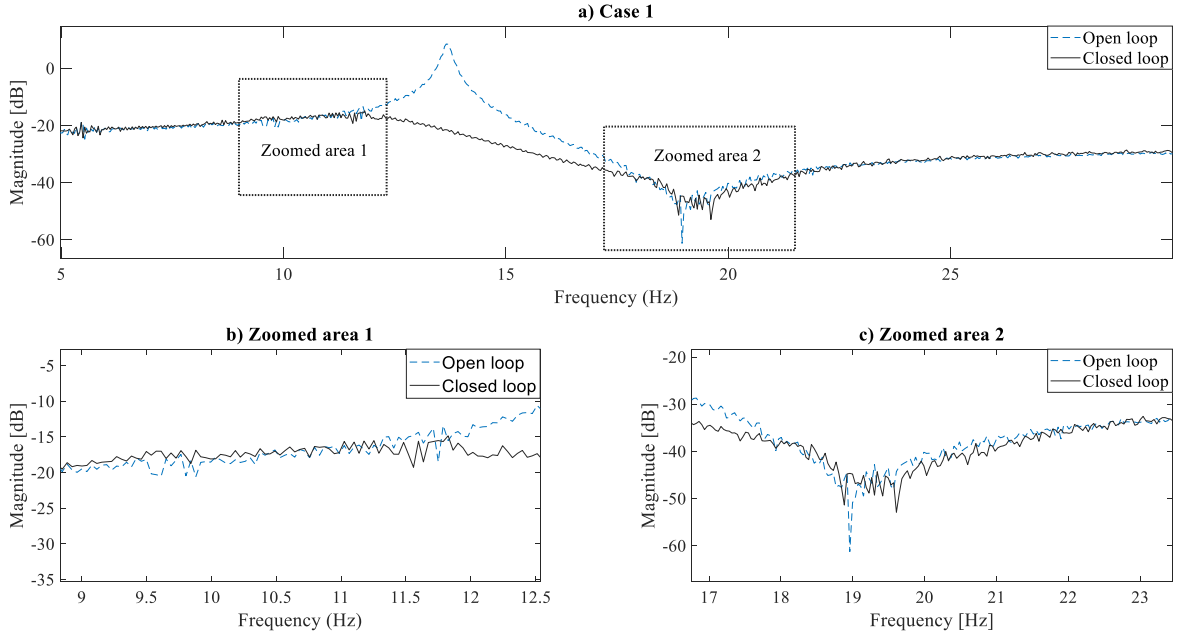


Fig. 16 (a) Frequency domain responses of the smart beam for Case 1; (b) Zoomed area 1; (c) Zoomed area

of 2 mm corresponding to 1.0 volt is applied on the tip of the piezo-beam. Therefore, the amplitude of the sensor signal starts decreasing from ±1.0 V. In this way, the free vibration is applied both in the uncontrolled and the controlled cases to the smart piezo-beam. It can easily be observed from the figure that the settling time is around 6.5 seconds for the open loop system. On the other hand, the designed controller manages to suppress the free vibrations of the smart beam with a settling time of nearly 0.56 seconds for each case.

In Fig. 14, time domain forced vibration responses of the smart beam is presented by also providing the controller output voltage values. In these experiments, the controller is switched on at the 10$^{th}$ second when the beam resonates at its first bending mode and kept active approximately 10 more seconds. The forced vibration suppression performance of the proposed controller is calculated in Eq. (48) (Turan *et al*. 2019) and is found as approximately 96% for all cases.

$$\text{Suppression rate} = \frac{[\text{Open loop magnitude}]_{\max} - [\text{Closed loop magnitude}]_{\max}}{[\text{Open loop magnitude}]_{\max}} \times 100 \tag{48}$$

Fig. 15 shows the responses in the frequency domain for five different cases. Accordingly, the designed controller is capable of effectively suppressing vibrations of the beam in the first resonance region. Approximately the same frequency response performances are obtained in all cases. The designed controller is capable of suppressing approximately 25 dB for all cases in the resonance region.

Fig. 16 shows the zoomed areas of the open and closed loop system responses in the frequency domain of the smart beam for Case 1. It is clear that the proposed controller is sensitive to both noise and perturbations and it desires to follow the reference in each case. Similar responses are also observed for all 5 cases.

## 6. Conclusions

In this research study, an LPV model-based gain scheduling $H_\infty$ controller is designed to suppress the free and forced vibrations of the smart beam. For this purpose, an original LPV model covering the frequencies in the range of all operating conditions is proposed and the gain-scheduling $H_\infty$ controller is designed by using the proposed LPV model. The servo arm position of the smart beam is choosen as scheduling parameter and additional compensator is not aimed for the performance increase. The proposed controller also focuses on suppressing the vibration of the smart beam which depends on the magnitude of the scheduling parameter. According to the results of the simulations and that of the experimental verifications obtained both in time and frequency domain, it is observed that the proposed controller is cable of successfully suppressing the free and the forced vibrations of the smart beam for different arm configurations at/around the first resonance frequency. The forced vibration suppression performance of the proposed controller is calculated and found as approximately 96% for all cases. The designed controller is also capable of suppressing approximately 25 dB for all cases in the resonance region. Moreover, the applied controller also performs the reference tracking of the open loop system in the frequency domain against noise for the five cases, sensitively by revealing the accuracy of the applied controller. The experimentally verified proposed design strategy has a huge potential for the usage of the isolation of the excessive vibrations on an aircraft wing structure experiencing a change in the weight of a payload in a particular time interval of the mission profile.

## References


Akın, O. (2015), "Active neuro-adaptive control of a smart beam having uncertainties in structural dynamics", Master Thesis; METU, Ankara, Turkey.

Akin, O and Sahin, M. (2017), "Active neuro-adaptive vibration suppression of a smart beam", *Smart Struct. Syst.*, *Int. J.*, **20**(6), 657-668. https://doi.org/10.12989/sss.2017.20.6.657

Alam, M.N. and Rahman, N.U. (2010), "Active vibration control of a piezoelectric beam using PID controller", *Experim. Study*, *Latin Am. J. Solids Struct.*, **9**(6), 657-673. https://doi.org/10.1590/S1679-78252012000600003

Algermissen, S., Rose, M., Keimer, R. and Sinapius, M. (2009), "Robust gain-scheduling for smart-structures in parallel robots", *Proceedings of the SPIE*, *Sensors and Smart Structures Technologies for Civil*, *Mechanical*, *and Aerospace Systems*, **7292**(86). https://doi.org/10.1117/12.810977

Avsar, A.L. and Sahin, M. (2016), "Bimorph piezoelectric energy harvester structurally integrated on a trapezoidal plate", *Smart Struct. Syst.*, *Int. J.*, **18**(2), 249-265. https://doi.org/10.12989/sss.2016.18.2.249

Boyd, S., El Ghaoui, L., Feron, E. and Balakrishnan, V. (1994), *Linear Matrix Inequalities in System and Control Theory*, Siam, PA, USA.

Chhabra, D., Narwal, K. and Singh, P. (2012), "Design and analysis of piezoelectric smart beam for active vibration control", *Int. J. Adv. Res. Technol.*, **1**(1), 1-5.

Khot, S.M., Yelve, N.P., Tomar, R., Desai, S. and Vittal, S. (2012), "Active vibration control of cantilever beam by using PID based output feedback controller", *J. Vib. Control*, **18**(3), 366-372. https://doi.org/10.1177/1077546311406307

Kumar, S., Srivastava, R. and Srivastava, R.K. (2014), "Active vibration control of smart piezo cantilever beam using PID controller", *Int. J. Res. Eng. Technol.*, **3**(1), 392-399. https://doi.org/10.22153/kej.2017.08.005

Omidi, E. and Mahmoodi, S.N. (2014), "Vibration control of collocated smart structures using $H_\infty$ modified positive position and velocity feedback", *J. Vib. Control*, **22**(10), 2434-2442. https://doi.org/10.1177/1077546314548471

Onat, C. (2015), "WGC based robust and gain scheduling PI controller design for condensing boilers", *Adv. Mech. Eng.*, **6**, p. 659051. https://doi.org/10.1155/2014/659051

Onat, C., Kucukdemiral, I.B., Sivrioglu, S. and Yuksek, I. (2007), "LPV model based gain scheduling controller for a full vehicle active suspension system", *J. Vib. Control*, **13**, 1629-1666. https://doi.org/10.1177/1077546307078784

Onat, C., Sahin, M. and Yaman, Y. (2011a), "Active vibration suppression of a smart beam by using an LQG control algorithm", *Proceedings of the 2nd International Conference of Engineering Against Fracture* (*ICEAF II*), Mykonos, Greece, June.

Onat, C., Sahin, M., Yaman, Y., Prasad, S. and Nemana, S. (2011b), "Design of an LPV based fractional controller for the vibration suppression of a smart beam", *International Workshop on Smart Materials&Structures and NDT in Aerospace*, Montreal, Canada, November.

Onat, C., Sahin, M. and Yaman, Y. (2012), "Fractional controller design for suppressing smart beam vibrations", *Aircraft Eng. Aerosp. Technol.*, **84**(4), 203-212. https://doi.org/10.1108/00022661211237728

Onat, C., Sahin, M. and Yaman, Y. (2017), "Gain scheduling $H_\infty$, control of a smart beam with parameter varying", In: *VIII ECCOMAS Thematic Conference on Smart Structures and Materials Smart*, Madrid, Spain, June.

Onat, C., Kucukdemiral, I.B., Sivrioglu, S., Yuksek, I. and Cansever, G. (2019), "LPV gain scheduling controller design for a nonlinear quarter-vehicle active suspension system", *Transact. Inst. Measur. Control*, **31**(1), 71-95. https://doi.org/10.1177/0142331208090630

Oveisi, A. and Nestorović, T. (2014), "Robust mixed $H_2/H_\infty$ active vibration controller in attenuation of smart beam", *Facta Universitatis*, *Series*: *Mechanical Engineering* **12**(3), 235-249.

Ros, N.F.M., Saad, M.S. and Darus, I.Z.M. (2015), "Dynamic modeling and active vibration control of a flexible beam: a review", *Int. J. Eng. Technol.*, **15**(5), 12-17.

Saad, M.S., Jamaluddin, H. and Darus, I.Z.M. (2012), "Active vibration control of flexible beam using differential evolution optimisation", *World Academy of Science and Technology*, **6**(2), 419-426. https://doi.org/10.5281/zenodo.1081515

Sahin, M., Karadal, F.M., Yaman, Y., Kircali, O.F., Nalbantoglu, V., Ulker, F.D. and Caliskan, T. (2008), "Smart structures and their applications on active vibration control: studies in the department of aerospace engineering", *Middle East Technical University*, *Journal of Electroceramics*, **20**(3-4), 167-174. https://doi.org/10.1007/s10832-007-9130-6

Sensor Technology, (2020), https://sensortechcanada.com/

Shouwei, G., Zhiyuan, G., Yong, S., Jincong, Y. and Xiaojin, Z. (2010), "Performance analysis and comparison of FXLMS and FULMS algorithm for active structure vibration control", *Proceedings of International Conference of Advance Computer Control*, **1**, pp. 197-201.

Speedgoat Educational Real-Time Target Machine, (2020), https://www.speedgoat.com/products-services

Turan, A., Onat, C. and Sahin, M. (2019), "Active vibration suppression of a smart beam via PID controller designed through weighted geometric center method", *Proceedings of the 10th Ankara International Aerospace Conference*, METU, Ankara, Turkey, September.

Zorić, N.D., Simonović, A.M., Mitrović, Z.S., Stupar, S.N., Obradović, A.M. and Lukić, N.S. (2014), "Free vibration control of smart composite beams using particle swarm optimized self-tuning fuzzy logic controller", *J. Sound Vib.*, **333**(21), 5244-5268. https://doi.org/10.1016/j.jsv.2014.06.001

*CC*